ACS Energy Letters

http://pubs.acs.org/journal/aelccp

On-Demand Solar and Thermal Radiation Management Based on Switchable Interwoven Surfaces

Yujie Ke, Yanbin Li, Lichen Wu, Shancheng Wang, Ronggui Yang, Jie Yin,* Gang Tan,* and Yi Long*

Cite This: *ACS Energy Lett.* 2022, 7, 1758−1763

Read Online

ABSTRACT: On-demand and selective regulation of the radiative cooling (long-wave infrared, LWIR) and solar heat gain (ultraviolet-, visible- and near-IR, UV−vis−NIR) of building facades is a grand challenge but essential to decrease energy usage in buildings. Here, we report a reconfigurable interwoven surface that can dynamically switch the overlapping sequence to achieve spectral selectivity and ultrabroadband modulations for windows, walls/roofs with decent spectral modulations, and energy-saving performance. The result surpasses the best reported passive radiative cooling smart windows with a more than doubled visible transmittance (T_{lum} = 0.50) and LWIR modulation ($\Delta\ \varepsilon_{LWIR}$ = 0.57). Our energy-saving samples outperform the commercial building materials across climate zones 2−6. This design principle is scalable and applicable for diverse materials, interwoven structures, and 2D-3D surfaces, which provide a strategy to give programmable heating/cooling modulations in various applications.

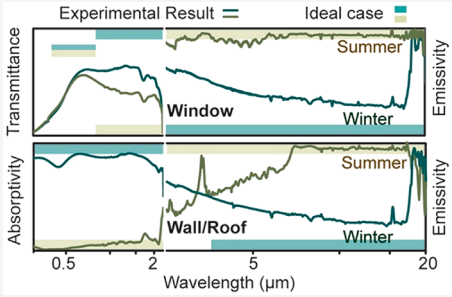

Buildings account for ∼51% of electricity and ∼33% of black carbon emission globally, which is expected to increase with modernization.[1,2] In developed regions such as the United States and European Union, up to ∼40% of the primary source of energy is consumed in buildings.[1,2] Building facades undergo heat exchange with outer space via radiative cooling (RC) and gain solar heat from the sun. RC cools the buildings through radiating heat in the form of long-wave near-infrared (LWIR, 2.5−20 μm) to the cold outer space, while the sun heats the buildings by absorbing ultraviolet−visible−near-infrared (UV−vis−NIR) light.[3−8] Modulation of both the RC and solar heat gain is desirable to reduce all-year-round energy consumption,[7−9] and the efficiency has been demonstrated by changing the roof materials via rotor[10] or flipping window.[6]

However, ultrabroadband modulation is always an inevitable challenge, and the spectral selectivity in building components differs. For example, compared with walls/roofs, windows need to have high luminous transparency to save lighting.[11−14] The reported approaches for the spectral tunability and selectivity are limited by the intrinsic material properties, such as using the phase-change materials[7] and mechano-/electrochromic devices.[15,16] There is a lack of an efficient and universal method to provide a design rule for different applications, including building windows, walls/roofs, and beyond. A programmable surface could be a different strategy to address some of those issues.

Mechanically reconfigurable structures[17,18] are known for their subtle designs of structural architectures with spatial rearrangement of 2D-3D blocks, leading to unique physical properties, which have been used in broad applications.[19−22] To maximize the ultrabroadband modulation for various heating/cooling demands, we design a dynamically tunable interwoven architecture with switchable overlaying sequences. It demonstrates a high spectra selectivity and modulation, as well as a high energy-saving performance for walls/roofs and windows in different climate conditions. Such a universal design could be extended to diverse materials, multidimensional switchable surfaces, and multiple scales that could be used but not limited to thermal management applications in buildings.

The switchable architected surface for modulating heating/cooling demands is constructed from perpendicularly weaved belts (x-y plane), giving packed and overlapped building blocks (Figure 1a). Each block can be designed to perform cooling or heating functionality by engineering its UV−vis−NIR-LWIR optical response (see calculation details in Note S1). The surface formed by these blocks can be switched, for example, by sliding

Received: February 21, 2022
Accepted: March 24, 2022

https://doi.org/10.1021/acsenergylett.2c00419
ACS Energy Lett. 2022, 7, 1758−1763

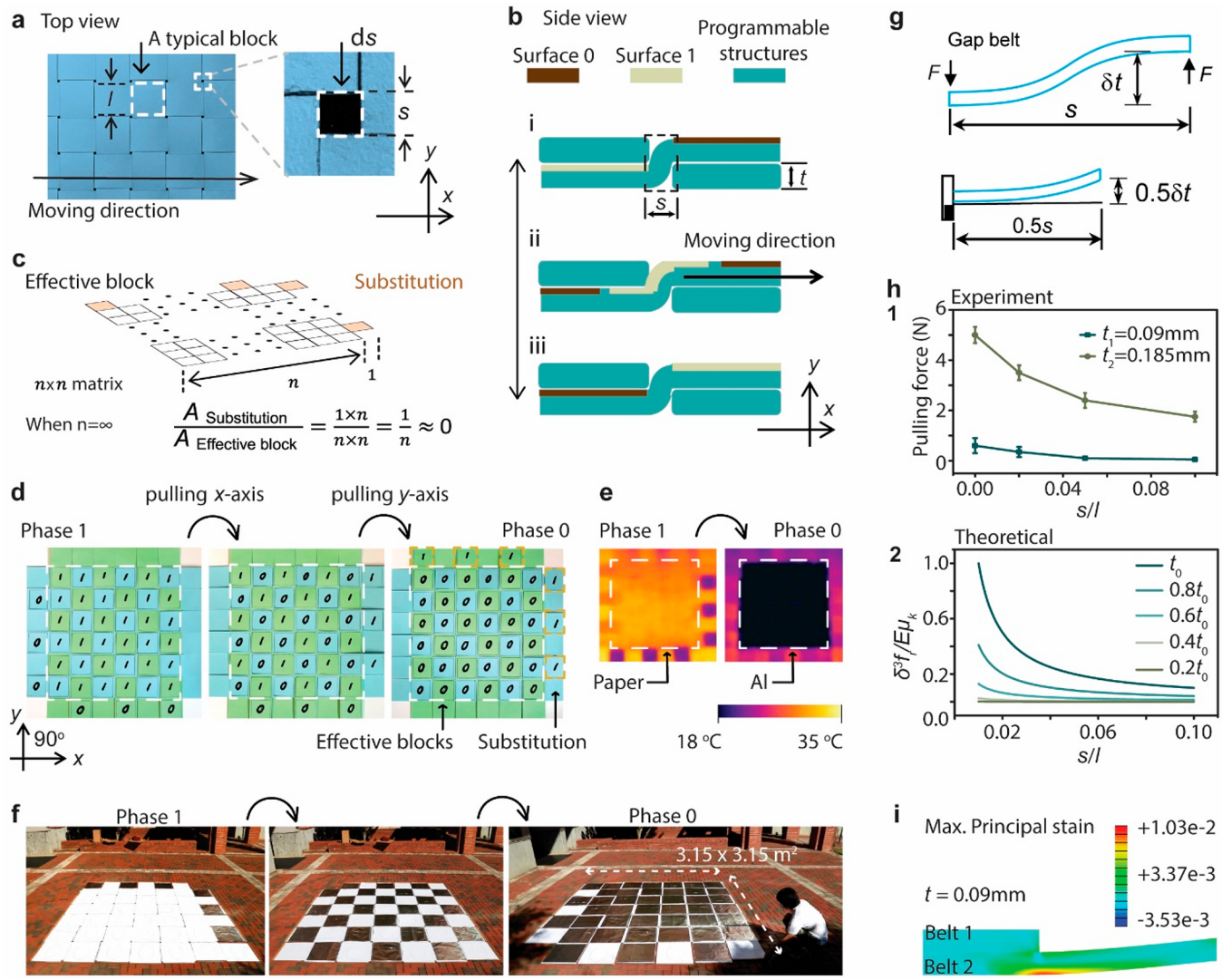

Figure 1. Design principle of the switchable surface. (a) Top-view schematic of the surface design with typical geometry parameters and the switchable principle along the *x*-axis as an example. (b) Side-view schematic of the switchable surface during the pulling process with a position exchange between surfaces 0 and 1. (c) Illustration of the "effective blocks" and "substitution" for an $n \times n$ surface and the area ratio of them. (d) Photographs to demonstrate a complete phase 0−1 transition by pulling the *x*- (blue paper) and *y*- (green paper) belts. (e) IR images to demonstrate a complete transition from paper-based high ε_{LWIR} to Al-based low ε_{LWIR} surfaces. The samples are heated on an ∼30 °C hot plate. (f) Demonstration of the surface transition in a meter-scale Al-paper sample. (g) Simplified beam model. (h) Experimental (1) and theoretical (2) analyses of the s/l ratio to the pulling force for samples with different thicknesses. (i) Nominal strain distribution contour.

the *x*-belts (belts along the *x*-axis) horizontally for one block distance (Figure 1ai); consequently, the spectra can be tuned and selected for potential ultrabroadband modulation. A side-view schematic is presented for two adjacent blocks to better illustrate the principle (Figure 1b). During the pulling process, the originally exposed block (denoted as surface 0, e.g., for heating) on top slides along the moving direction and becomes concealed (Figure 1bi,ii), while the block underneath (denoted as surface 1, e.g., for cooling) shifts to the right and becomes fully exposed (Figure 1biii). The process leads to the architected surface changing in blocks from 0 to 1 for all *x*-belts, which counts for half of the surface. A fully 0-to-1 switchable surface is achievable by repeating the process for all the *y*-belts. The successful production of the surface requires two types of blocks: the effective blocks and the substitution highlighted in white and orange, respectively (Figure 1c). In each pull, only the effective blocks take effect with the substitution hidden. The area ratio between the effective blocks and substitution is calculated to be $1/n$ for an $n \times n$ matrix (Figure 1c), eliminating the extra requirement for storing the substitution in the methods such as simply changing the surface materials.[10]

We first experimentally demonstrate the proof of concept of switchable interwoven surfaces using green and blue paper sheets with equidistant parallel cuts along the *x*- and *y*-axes with premarked 1 and 0 (Figure S2a). These two components are assembled perpendicularly along the *x*- and *y*-axes, forming an architected surface with all the effective building blocks showing surface 1 (Figure 1d). We denote this state as phase 1. After sequentially pulling along the *x*-axis followed by the *y*-axis, the entire surface can transit from phase 1 to 0 with all the effective building blocks showing surface 0 (Figure 1d). We can use the matrices A_k (k is an integer) to accurately describe all combinatorial phases (Note S2) of the switchable architected surface. The switching process between two different phases represented by two matrices A_l and A_k can be mathematically expressed as $A_l = T_{lk}A_k$, where T_{lk} represents the geometrical

https://doi.org/10.1021/acsenergylett.2c00419
ACS Energy Lett. 2022, 7, 1758−1763

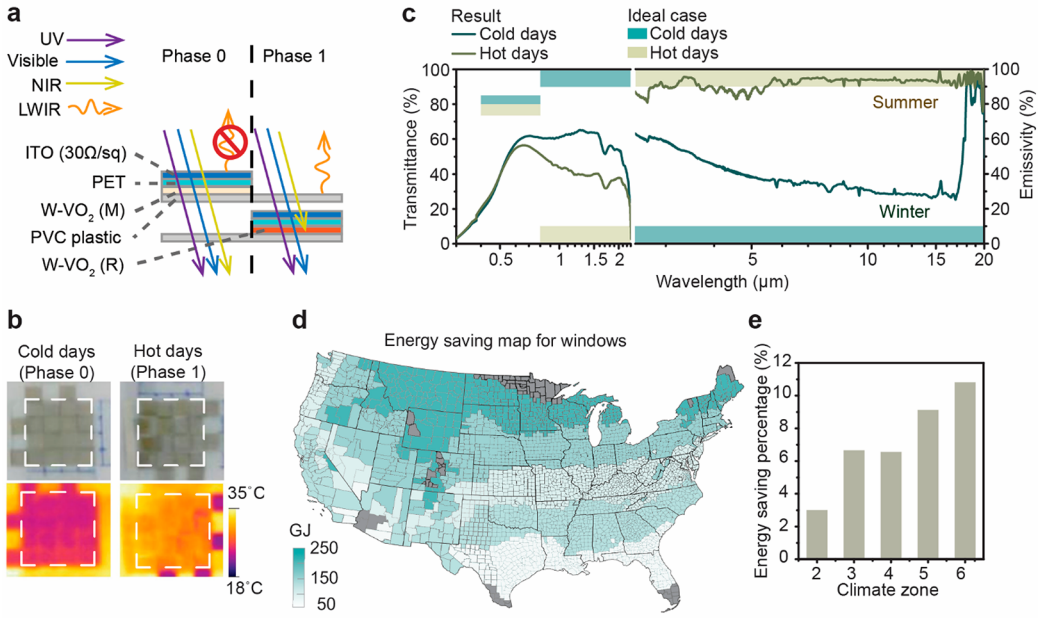

Figure 2. (a) Schematic of the ITO/VO_2/PVC sample design for windows. Phases 0 and 1 are for cold and hot days, respectively. (b) Photographs and corresponding thermal images of the ITO/VO_2/PVC sample on the two phases. Effective areas are marked by the dashed lines. (c) Ideal cases and experimental spectrum performance of the ITO/VO_2/PVC sample. (d,e) Annually estimated HVAC (d) energy-saving potential in the United States and (e) energy-saving percentage in zones 2−6 (ii) using the ITO/VO_2/PVC sample. Alaska and Hawaii are mostly beyond climate zones 2−6 and are not included here.

transformation including translation and rotation (Note S2 and Figure S1).

We demonstrate the switchable LWIR emissivity (ε_{LWIR}) functionality by differentiating the two phases using aluminum (Al) foil (ε_{LWIR} = ∼0.1) and white paper (ε_{LWIR} = ∼0.93) as an example (Figure 1e). The surface is observed to gradually transform from an Al foil- to a white paper-covered surface, the corresponding infrared (IR) images of which show a transition from a dark low-ε_{LWIR} (phase 0) to a bright high-ε_{LWIR} (phase 1) state (Figure S2 and Video S1). We further demonstrate that this concept can be readily upscaled to a meter-scale sample with an effective area of 2.8 m × 2.8 m (Figure 1f and Video S2).

To evaluate the pulling force needed for actuating the dynamic switching, we conduct tensile tests (Figure S3) and develop a simplified mechanics model (Figure 1g and Note S3) to reveal the quantitative relationship between the force and the geometry of the interwoven belt structure. It shows an approximately constant pulling force during the dynamic switch on samples made of paper or PVC-based plastic foils (Figure S4). The pulling force for actuating the surface switch is mainly determined by the belt thickness t (Figure 1b) and the ratio of gap length s to belt width l (Figure 1a), i.e., s/l. s/l also determines the surface porosity of the gaps between belts, which can be negligible (less than 1%) even for a large gap with $s/l = 0.1$ (Figure S3) and thus provide an excellent surface coverage for heating/cooling modulation. The pulling force can be reduced by decreasing t and/or increasing s/l (Figure 1h and Figure S5). For example, for a typical paper-based belt, as the t is reduced by half from 0.185 to 0.09 mm, the pulling force can drop by 10-fold, i.e., reducing from ∼5 to 0.5 N for the design with $s/l = 0.02$ (Figure 1h1). At constant t (t = 0.185 mm), as s/l increases from 0.02 to 0.1, the pulling force is reduced by nearly half from about 5 to 2.5 N. This is consistent with the analytical model (Figure 1h2). Despite the stress concentrates at the two ends of the gap section (Figure S6), the local maximum principal strain is ∼1% in the paper-based design, lower than the elastic strain limit (Figure 1i). When scaling up the design, as l increases from 8 to 30 mm, the pulling force decreases (Figure S7). For the meter-scale sample with l ∼ 0.45 m in Figure 1f, only a small pulling force as low as ∼1.8 N is needed for actuating the mechanical switching (Video S3), indicating its promising application and actuation on large scales.

In the following section, we designed the interwoven surface with suitable materials and demonstrate their potential for energy-saving window and roof application. Windows are one of the least energy-efficient and most complicated parts of buildings.[7] We produce the sample consisting of the functional layers of ITO, tungsten-doped vanadium dioxide (VO_2), and PVC plastic foil in sequence (denoted as ITO/VO_2/PVC) (Figures 2a and S8a−d). In phase 0 for cold days (Figure 2a), the solar energy (UV−vis−NIR) passes all layers for heating due to the high transparency of the materials in each layer. The LWIR emission remains low since the exposure of low-ε ITO (30Ω/sq) is on the top surface. Once switching to phase 1 for hot days (Figure 2a), the NIR solar energy is blocked by the VO_2 layer due to the temperature-induced crystal transition from monoclinic to rutile VO_2.[23] The optical transition of VO_2 is preserved in the transparent matrix, and detailed optical investigations can be found in previous reports.[21,24−26] The LWIR emission changes to high state by switching the high-ε PVC-based plastics on top. The sample exhibits a dark and a bright IR image on phases 0 and 1, respectively, accompanied by a consistent transparent yellow-brown color (Figure 2b). An ideal energy-saving single pane window needs to maintain all-year visible transparency, a low ε_{LWIR}, and a high NIR transmittance on cold days, as well as a reversed response on hot days (Figure 2c).[7] Our sample exhibits a constant luminous transmission (T_{lum}) of 0.50 ± 0.02 on both phases (Figure 2c), while they perform reversely on the NIR-LWIR spectra. The solar transmittance in the NIR region (T_{NIR}) increases from 0.41

https://doi.org/10.1021/acsenergylett.2c00419
ACS Energy Lett. 2022, 7, 1758−1763

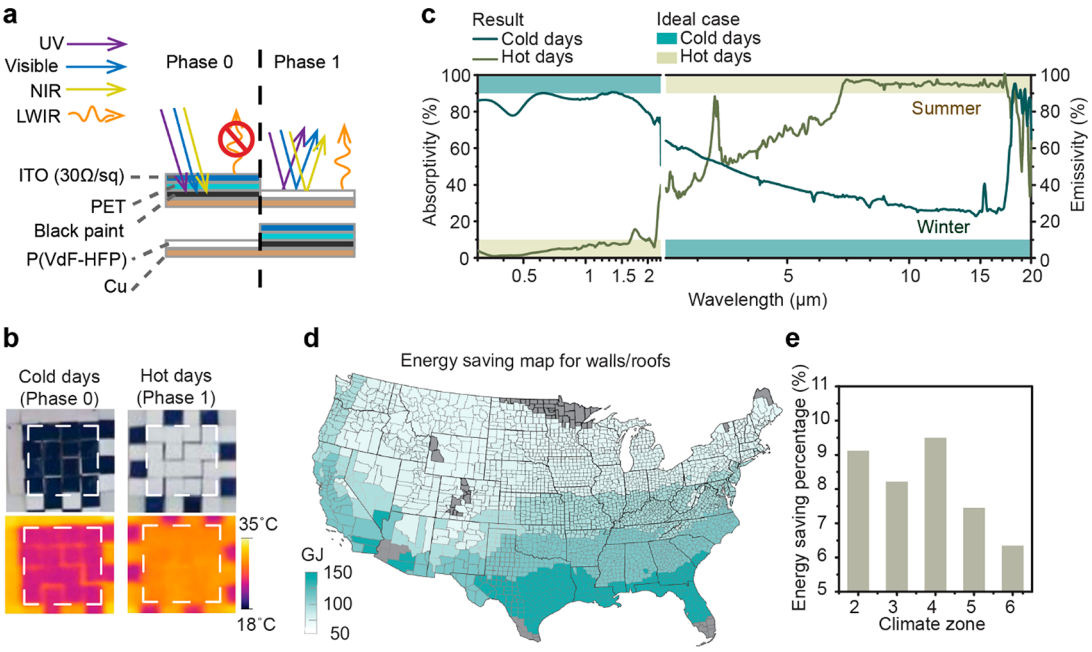

Figure 3. (a) Schematic of the ITO/BP/PVDF-HFP sample for walls/roofs. Phases 0 and 1 are for cold and hot days, respectively. (b) Photographs and corresponding thermal images of the ITO/BP/PVDF-HFP sample on the two phases. Effective areas are marked by the dashed lines. (c) Ideal cases and experimental spectrum performance of the ITO/BP/PVDF-HFP sample. (d,e) Annually estimated HVAC energy-saving potential (d) and percentage (e) in climate zones of 2−6 in the United States using the ITO/BP/PVDF-HFP sample for walls/roofs. Alaska and Hawaii are mostly beyond climate zones 2−6 and are not included here.

± 0.02 to 0.59 ± 0.02, and the ε_{LWIR} decreases from 0.93 ± 0.02 to 0.36 ± 0.02 during the transition from phase 1 to 0 (Figure 2c). The method effectively addresses the limitation of the RC-regulated smart window,[7] giving more than doubled T_{lum} (0.50 vs 0.22) and Δ ε_{LWIR} (0.57 vs 0.23) (Note S1).

The energy-saving simulation is conducted using the same medium office building (Figure S9) from climate zones 2−6 in the United States (Table S1). We compare the window sample against the commercial glass (Table S2) with fixed T_{sol} = 0.5 and ε_{LWIR} = 0.84 (Figure S10). The ITO/VO_2/PVC sample shows overall total energy savings from zones 2 to 6 in typical US cities with up to 214 GJ energy savings (Figure 2d) and 10.8% in zone 6 (Figure 2e). By examining the monthly energy savings, our sample saves more energy in both cold and warm seasons: e.g., in zone 6, the sample gives an energy savings of 42 GJ in January and 4 GJ in July (Figure S10). The monthly energy savings across 5 climate zones in all seasons suggest that by tuning both ε_{LWIR} and T_{NIR} favorably, the energy could be saved through windows in both winter and summer seasons.

We further modified the programmable interwoven surface and demonstrate their potential for energy-saving walls/roofs. We produce the sample consisting of indium tin oxide (ITO), black paint (BP), and porous poly(vinylidene fluoride-hexafluoropropylene) (PVDF-HFP) functional layers in sequence to approach the ideal modulation surface (denoted as ITO/BP/PVDF-HFP) (Figures 3a and S9e−h). In phase 0 (cold days) (Figure 3a), the solar energy (UV−vis−NIR) passes through the transparent ITO (30Ω/sq) and PET layers and then is absorbed by the black paint for heating, while the LWIR emission remains low since the low-ε ITO layer (30Ω/sq) is on the top surface. In phase 1 (hot days) (Figure 3a), the top layer of porous PVDF-HFP (Figure S9h) shows a strong reflectance to solar (UV−vis−NIR) and a high-ε for radiative cooling. Phase 1 has a white high-reflectance appearance, and phase 0 shows a high-absorbance black color; while phase 1 displays a brighter IR image than phase 0 (Figure 3b). The design principle for walls/roofs needs to be as follows (Figure 3c): A high ε_{LWIR} to promote RC and low solar absorption (A_{sol}) to reduce heat gain are needed on hot days to cool the buildings, and a reverse spectrum is required on cold days. Our sample shows a high ε_{LWIR} (0.91 ± 0.03) and a low A_{sol} (0.05 ± 0.01) for phase 1 and switches to a reverse performance for phase 0 with a reduced ε_{LWIR} (0.38 ± 0.03) and a high A_{sol} (0.87 ± 0.01) (Figure 3c), which is consistent with the desired modulation manner of energy-saving walls/roofs.

To analyze the energy-saving performance, we conduct the simulation using the same medium office building (Figure S10). The produced ITO/BP/PVDF-HFP for walls/roofs is benchmarked with commercial products (e.g., stucco and roofing membrane) with fixed optical properties (Table S3). The ITO/BP/PVDF-HFP sample gives all-year energy savings in climate zones 2−6 in the United States (Figures 3d and S11) and the highest total HVAC energy savings up to 137 GJ in climate zone 2 (Figure 3d) and 9.5% in zone 4 (Figure 3e). Our sample outperforms the commercial walls/roofs in both cold and warm seasons: e.g., in zone 2, it shows ∼5 and ∼18 GJ less energy in January and July (Figure S11).

The two demonstrations show great potential in the interwoven structure to solve one of the biggest challenges for the building facades: the high-performance spectral modulation on the ultrabroad bands. Both demonstrations are based on switching emissivity mechanically. Further improvement is necessary for practical application, such as thermal conductivity, cost, durability, and abrasion loss of materials. Thermal conductivity can be improved using the thin and thermally conductive materials and/or applying an electrostatic force to enhance contact as being reported previously.[10] The VO_2 is expected to have a service life of ∼16−33 years if it is well encapsulated to prevent water and oxygen.[27−29] Reducing the friction can improve the durability and reduce abrasion loss of

https://doi.org/10.1021/acsenergylett.2c00419
ACS Energy Lett. 2022, 7, 1758−1763

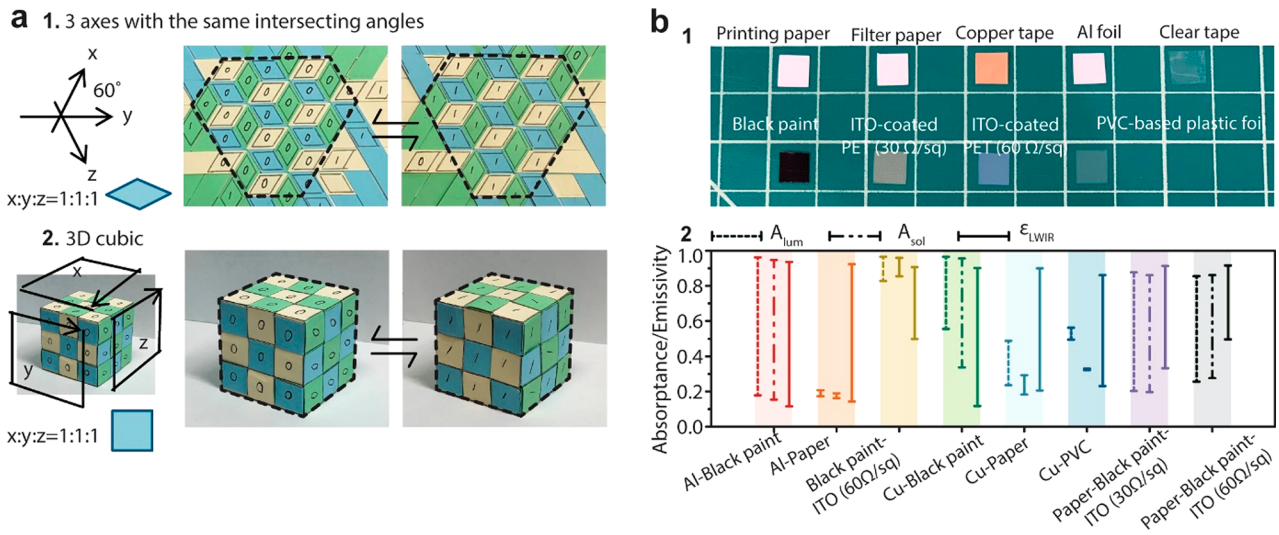

Figure 4. (a) Photographs of the modified weaving architectures with 2D 3-axes (1) and a 3D cubic design (2). The axis arrangement, ratio of the belt width, and block morphology are illustrated on the right. The effective areas are indicated by dashed lines. (b) Photographs of the raw materials to produce switchable surfaces (1) and the performance summary of 8 surfaces (2).

materials, and potential improvement methods can reduce the layer thickness and increase the gap size as demonstrated in Figures 1h and S5.

Moreover, the design rule of the interwoven surface is universally applicable to diverse structural and material designs. We develop 6 more structures (Figures 4a and S12) for inspiration by controlling 1) the width ratios of belts for each axis, 2) the intersect angle among the axes, and 3) the number of axes, including the equilateral 3-axes (Figure 4a1) and the 3-D cubic structures (Figure 4a2). Besides the aforementioned materials, we also explore 8 more combinations (Figure S13) using commercially available materials as inspiring examples (Figure 4b1). Their tunable spectra are detailed in Figure S13, and the absorption/emission tunability is summarized in Figure 4b2.

In summary, we present a programmable interwoven surface that can dynamically switch the overlapping sequence to achieve high spectral selectivity and ultrabroadband modulations (UV-to-LWIR). We design two structures to meet the energy-saving demands for building windows and walls/roofs. The spectral performance significantly surpasses the best-reported result of radiative cooling regulated smart windows. Both designed wall/roof and window samples outperform the counterpart commercial building materials across climate zones 2−6. The method is universal, scalable, and applicable for different spectral-selective and ultrabroadband modulations, which provide a design rule for further customization and improvement with multiple scales to be utilized in various spectral modulation applications.

■ ASSOCIATED CONTENT

Supporting Information

The Supporting Information is available free of charge at https://pubs.acs.org/doi/10.1021/acsenergylett.2c00419.

Materials synthesis and characterization, mechanical theory and analysis, calculation of solar and thermal performance, energy simulation details, and data for universal demonstration of materials and structures (PDF)

Video S1 (MP4)

Video S2 (MP4)

Video S3 (MP4)

■ AUTHOR INFORMATION

Corresponding Authors

Yi Long − *School of Materials Science and Engineering, Nanyang Technological University, Singapore 639798, Singapore; Singapore-HUJ Alliance for Research and Enterprise (SHARE), Campus for Research Excellence and Technological Enterprise (CREATE), Singapore 138602, Singapore; Sino-Singapore International Joint Research Institute (SSIJRI), Guangzhou 510000, China;* orcid.org/0000-0003-0608-8253; Email: longyi@ntu.edu.sg

Gang Tan − *Department of Civil and Architectural Engineering, University of Wyoming, Laramie, Wyoming 82071, United States;* orcid.org/0000-0001-5349-4110; Email: gtan@uwyo.edu

Jie Yin − *Department of Mechanical and Aerospace Engineering, North Carolina State University, Raleigh, North Carolina 27695, United States*; Email: jyin8@ncsu.edu

Authors

Yujie Ke − *School of Materials Science and Engineering, Nanyang Technological University, Singapore 639798, Singapore*

Yanbin Li − *Department of Mechanical and Aerospace Engineering, North Carolina State University, Raleigh, North Carolina 27695, United States*

Lichen Wu − *Department of Civil and Architectural Engineering, University of Wyoming, Laramie, Wyoming 82071, United States*

Shancheng Wang − *School of Materials Science and Engineering, Nanyang Technological University, Singapore 639798, Singapore*

Ronggui Yang − *State Key Laboratory of Coal Combustion, School of Energy and Power Engineering, Huazhong University of Science and Technology, Wuhan 430074, China;* orcid.org/0000-0002-3602-6945

Complete contact information is available at: https://pubs.acs.org/10.1021/acsenergylett.2c00419

https://doi.org/10.1021/acsenergylett.2c00419
ACS Energy Lett. 2022, 7, 1758−1763

Author Contributions

Y.K. and Y.L. contributed equally. Y.L. proposed and guided the project as Principal Investigator. Y.L., J.Y., and G.T. contributed to the detailed design of experiments and simulations. Y.K. conducted the experiments for material design, preparation, and analysis. Y.L. conducted the mechanical experiment, simulation, and analysis and prepared the samples in the videos. L.W. and G.T. conducted the energy simulation and analysis. S.W. conducted data analysis for energy savings. Y.K., Y.L., Y.J., G.T., and Y.L. drafted, discussed, and revised the manuscript. All authors checked the manuscript.

Notes

The authors declare the following competing financial interest(s): A Singapore provisional patent (10202108396V) related to this work has been filled by Y.L. and Y.K.

■ ACKNOWLEDGMENTS

The research was supported by the National Research Foundation, Prime Minister's Office, Singapore, under its Campus for Research Excellence and Technological Enterprise (CREATE) program and the Singapore-HUJ Alliance for Research and Enterprise (SHARE), Minister of Education (MOE) Academic Research Fund Tier 1 RG103/19 (S), RG86/20, and RG71/21, and the Sino-Singapore International Joint Research Institute (SSIJRI). J.Y. would like to thank the National Science Foundation for grant numbers CMMI-2005374 and CMMI-2013993.

■ REFERENCES

(1) Berardi, U. A Cross-Country comparison of the Building Energy Consumptions and Their Trends. *Resour., Conserv. Recycl.* **2017**, *123*, 230−241.

(2) IPCC, Intergovernmental Panel on Climate Change. *Climate Change 2014: Mitigation of Climate Change*; Chapter 9: Buildings, 2014.

(3) Hsu, P.-C.; Li, X. Photon-Engineered Radiative Cooling Textiles. *Science* **2020**, *370*, 784.

(4) Mandal, J.; Fu, Y.; Overvig, A. C.; Jia, M.; Sun, K.; Shi, N. N.; Zhou, H.; Xiao, X.; Yu, N.; Yang, Y. Hierarchically Porous Polymer Coatings for Highly Efficient Passive Daytime Radiative Cooling. *Science* **2018**, *362*, 315.

(5) Raman, A. P.; Anoma, M. A.; Zhu, L.; Rephaeli, E.; Fan, S. Passive Radiative Cooling Below Ambient Air Temperature under Direct Sunlight. *Nature* **2014**, *515*, 540−544.

(6) Wang, S.; Zhou, Y.; Jiang, T.; Yang, R.; Tan, G.; Long, Y. Thermochromic Smart Windows with Highly Regulated Radiative Cooling and Solar Transmission. *Nano Energy* **2021**, *89*, 106440.

(7) Wang, S.; Jiang, T.; Meng, Y.; Yang, R.; Tan, G.; Long, Y. Thermochromic Smart Windows with Radiative Cooling Regulation. *Science* **2021**, *374*, 1501−1504.

(8) Tang, K.; Dong, K.; Li, J.; Gordon Madeleine, P.; Reichertz Finnegan, G.; Kim, H.; Rho, Y.; Wang, Q.; Lin, C.-Y.; Grigoropoulos Costas, P.; Javey, A.; Urban Jeffrey, J.; Yao, J.; Levinson, R.; Wu, J. Temperature-Adaptive Radiative Coating for All-Season Household Thermal Regulation. *Science* **2021**, *374*, 1504−1509.

(9) Li, X.; Xie, W.; Sui, C.; Hsu, P.-C. Multispectral Thermal Management Designs for Net-Zero Energy Buildings. *ACS Materials Lett.* **2020**, *2*, 1624−1643.

(10) Li, X.; Sun, B.; Sui, C.; Nandi, A.; Fang, H.; Peng, Y.; Tan, G.; Hsu, P.-C. Integration of Daytime Radiative Cooling and Solar Heating for Year-Round Energy Saving in Buildings. *Nat. Commun.* **2020**, *11*, 6101.

(11) Eh, A. L.-S.; Chen, J.; Zhou, X.; Ciou, J.-H.; Lee, P. S. Robust Trioptical-State Electrochromic Energy Storage Device Enabled by Reversible Metal Electrodeposition. *ACS Energy Lett.* **2021**, *6*, 4328−4335.

(12) Shao, Z.; Huang, A.; Ming, C.; Bell, J.; Yu, P.; Sun, Y.-Y.; Jin, L.; Ma, L.; Luo, H.; Jin, P.; Cao, X. All-Solid-State Proton-Based Tandem Structures for Fast-Switching Electrochromic Devices. *Nat. Electron.* **2022**, *5*, 45−52.

(13) Cai, G.; Chen, J.; Xiong, J.; Lee-Sie Eh, A.; Wang, J.; Higuchi, M.; Lee, P. S. Molecular Level Assembly for High-Performance Flexible Electrochromic Energy-Storage Devices. *ACS Energy Lett.* **2020**, *5*, 1159−1166.

(14) Ke, Y.; Chen, J. W.; Lin, C. J.; Wang, S. C.; Zhou, Y.; Yin, J.; Lee, P. S.; Long, Y. Smart Windows: Electro-, Thermo-, Mechano-, Photochromics, and Beyond. *Adv. Energy Mater.* **2019**, *9*, 1902066.

(15) Rao, Y.; Dai, J.; Sui, C.; Lai, Y.-T.; Li, Z.; Fang, H.; Li, X.; Li, W.; Hsu, P.-C. Ultra-Wideband Transparent Conductive Electrode for Electrochromic Synergistic Solar and Radiative Heat Management. *ACS Energy Lett.* **2021**, *6*, 3906−3915.

(16) Fang, H.; Xie, W.; Li, X.; Fan, K.; Lai, Y.-T.; Sun, B.; Bai, S.; Padilla, W. J.; Hsu, P.-C. A Triple-Mode Midinfrared Modulator for Radiative Heat Management of Objects with Various Emissivity. *Nano Lett.* **2021**, *21*, 4106−4114.

(17) Blees, M. K.; Barnard, A. W.; Rose, P. A.; Roberts, S. P.; McGill, K. L.; Huang, P. Y.; Ruyack, A. R.; Kevek, J. W.; Kobrin, B.; Muller, D. A.; McEuen, P. L. Graphene Kirigami. *Nature* **2015**, *524*, 204−207.

(18) Silverberg, J. L.; Evans Arthur, A.; McLeod, L.; Hayward Ryan, C.; Hull, T.; Santangelo Christian, D.; Cohen, I. Using Origami Design Principles to Fold Reprogrammable Mechanical Metamaterials. *Science* **2014**, *345*, 647−650.

(19) Li, S.; Deng, B.; Grinthal, A.; Schneider-Yamamura, A.; Kang, J.; Martens, R. S.; Zhang, C. T.; Li, J.; Yu, S.; Bertoldi, K.; Aizenberg, J. Liquid-Induced Topological Transformations of Cellular Microstructures. *Nature* **2021**, *592*, 386−391.

(20) Xia, X.; Afshar, A.; Yang, H.; Portela, C. M.; Kochmann, D. M.; Di Leo, C. V.; Greer, J. R. Electrochemically Reconfigurable Architected Materials. *Nature* **2019**, *573*, 205−213.

(21) Ke, Y.; Yin, Y.; Zhang, Q.; Tan, Y.; Hu, P.; Wang, S.; Tang, Y.; Zhou, Y.; Wen, X.; Wu, S.; White, T. J.; Yin, J.; Peng, J.; Xiong, Q.; Zhao, D.; Long, Y. Adaptive Thermochromic Windows from Active Plasmonic Elastomers. *Joule* **2019**, *3*, 858−871.

(22) Tang, Y.; Lin, G.; Yang, S.; Yi, Y. K.; Kamien, R. D.; Yin, J. Programmable Kiri-Kirigami Metamaterials. *Adv. Mater.* **2017**, *29*, 1604262.

(23) Ke, Y.; Zhang, B.; Wang, T.; Zhong, Y.; Vu, T. D.; Wang, S.; Liu, Y.; Magdassi, S.; Ye, X.; Zhao, D.; Xiong, Q.; Sun, Z.; Long, Y. Manipulating Atomic Defects in Plasmonic Vanadium Dioxide for Superior Solar and Thermal Management. *Mater. Horiz.* **2021**, *8*, 1700−1710.

(24) Li, S. Y.; Niklasson, G. A.; Granqvist, C. G. Nanothermochromics: Calculations for VO_2 Nanoparticles in Dielectric Hosts Show Much Improved Luminous Transmittance and Solar Energy Transmittance Modulation. *J. Appl. Phys.* **2010**, *108*, 063525.

(25) Li, S. Y.; Niklasson, G. A.; Granqvist, C. G. Nanothermochromics with VO_2-Based Core-Shell Structures: Calculated Luminous and Solar Optical Properties. *J. Appl. Phys.* **2011**, *109*, 113515.

(26) Ke, Y.; Zhang, Q.; Wang, T.; Wang, S.; Li, N.; Lin, G.; Liu, X.; Dai, Z.; Yan, J.; Yin, J.; Magdassi, S.; Zhao, D.; Long, Y. Cephalopod-Inspired Versatile Design Based on Plasmonic VO_2 Nanoparticle for Energy-Efficient Mechano-Thermochromic Windows. *Nano Energy* **2020**, *73*, 104785.

(27) Zhou, X.; Meng, Y.; Vu, T. D.; Gu, D.; Jiang, Y.; Mu, Q.; Li, Y.; Yao, B.; Dong, Z.; Liu, Q.; Long, Y. A New Strategy of Nanocompositing Vanadium Dioxide with Excellent Durability. *J. Mater. Chem. A* **2021**, *9*, 15618−15628.

(28) Chang, T.; Cao, X.; Li, N.; Long, S.; Zhu, Y.; Huang, J.; Luo, H.; Jin, P. Mitigating Deterioration of Vanadium Dioxide Thermochromic Films by Interfacial Encapsulation. *Matter* **2019**, *1*, 734−744.

(29) Vu, T. D.; Xie, H.; Wang, S.; Hu, J.; Zeng, X.; Long, Y. Durable Vandium Dioxide with 33-Year Service Life for Smart Window Applications. *Mater. Today Energy* **2022**, 100978.